

## CCN Spectra, Hygroscopicity, and Droplet Activation Kinetics of Secondary Organic Aerosol Resulting from the 2010 Deepwater Horizon Oil Spill

Richard H. Moore,<sup>†</sup> Tomi Raatikainen,<sup>‡</sup> Justin M. Langridge,<sup>§,||</sup> Roya Bahreini,<sup>§,||</sup> Charles A. Brock,<sup>§</sup> John S. Holloway,<sup>§,||</sup> Daniel A. Lack,<sup>§,||</sup> Ann M. Middlebrook,<sup>§</sup> Anne E. Perring,<sup>§,||</sup> Joshua P. Schwarz,<sup>§,||</sup> J. Ryan Spackman,<sup>§,⊥</sup> and Athanasios Nenes<sup>\*†,‡</sup>

<sup>†</sup>School of Chemical & Biomolecular Engineering, Georgia Institute of Technology, Atlanta, Georgia, United States

<sup>‡</sup>School of Earth & Atmospheric Sciences, Georgia Institute of Technology, Atlanta, Georgia, United States

<sup>§</sup>Earth System Research Laboratory, National Oceanic and Atmospheric Administration, Boulder, Colorado, United States

<sup>||</sup>Cooperative Institute for Research in Environmental Sciences, University of Colorado, Boulder, Colorado, United States and

<sup>⊥</sup>Science and Technology Corporation, Boulder, Colorado, United States

### Supporting Information

**ABSTRACT:** Secondary organic aerosol (SOA) resulting from the oxidation of organic species emitted by the Deepwater Horizon oil spill were sampled during two survey flights conducted by a National Oceanic and Atmospheric Administration WP-3D aircraft in June 2010. A new technique for fast measurements of cloud condensation nuclei (CCN) supersaturation spectra called Scanning Flow CCN Analysis was deployed for the first time on an airborne platform. Retrieved CCN spectra show that most particles act as CCN above  $(0.3 \pm 0.05)\%$  supersaturation, which increased to  $(0.4 \pm 0.1)\%$  supersaturation for the most organic-rich aerosol sampled. The aerosol hygroscopicity parameter,  $\kappa$ , was inferred from both measurements of CCN activity and from humidified-particle light extinction, and varied from 0.05 to 0.10 within the emissions plumes. However,  $\kappa$  values were lower than expected from chemical composition measurements, indicating a degree of external mixing or size-dependent chemistry, which was reconciled assuming bimodal, size-dependent composition. The CCN droplet effective water uptake coefficient,  $\gamma_{\text{cond}}$ , was inferred from the data using a comprehensive instrument model, and no significant delay in droplet activation kinetics from the presence of organics was observed, despite a large fraction of hydrocarbon-like SOA present in the aerosol.



### INTRODUCTION

The explosion and loss of the Deepwater Horizon (DWH) oil platform on 20 April 2010 resulted in the release of millions of barrels of oil into the waters of the Gulf of Mexico during April–July, 2010.<sup>1</sup> While a large portion of the oil-gas mixture remained dissolved or dispersed in the water column, a substantial portion reached the water surface and evaporated into the atmosphere over a period of hours to days.<sup>2,3</sup> Volatile organic carbon (VOC) and intermediate volatility organic carbon (IVOC) species are oxidized in the atmosphere, which lowers their volatility causing them to nucleate new particles or condense onto existing aerosol particles. Termed secondary organic aerosols (SOA), these particles are an important but uncertain contributor to adverse air quality and climate change.<sup>4,5</sup>

In this work, we present a detailed characterization of the hygroscopic and droplet-forming properties of SOA formed in

the vicinity of the DWH site during two survey flights conducted by the National Oceanic and Atmospheric Administration (NOAA) WP-3D aircraft on 8 and 10 June 2010. These survey flights provide a unique case study of hydrocarbon-derived SOA that has experienced relatively little atmospheric oxidative processing and whose concentrations exceed those of the more oxidatively aged organic aerosol background. Both fresh and aged SOA coexist in urban environments, although the latter species are usually much more abundant,<sup>6</sup> and hence, may obscure the influence of the former on measured cloud condensation nuclei (CCN) activation and droplet growth.

**Received:** September 24, 2011

**Revised:** February 8, 2012

**Accepted:** February 21, 2012

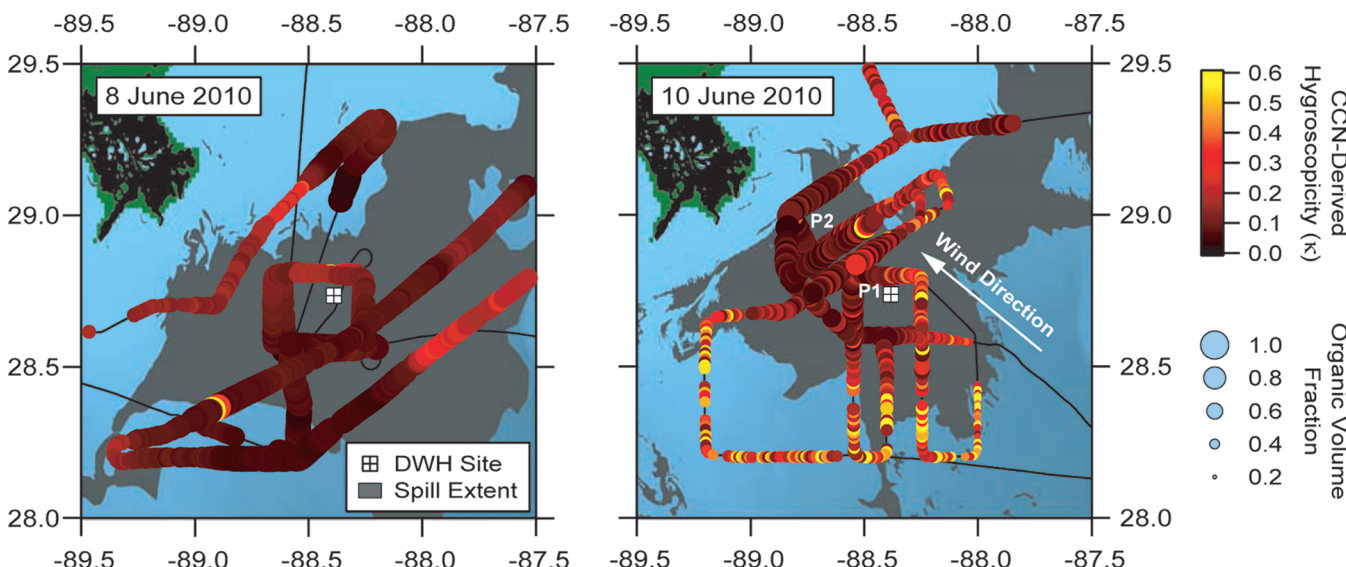


**Figure 1.** Aircraft trajectories for the survey flights on 8 June (left) and 10 June (right) when the aircraft was sampling near the DWH spill site. Markers are colored by the CCN-derived hygroscopicity and sized by the aerosol organic volume fraction. The gray shaded area represents the satellite-derived extent of surface oil (both fresh and aged).<sup>8</sup> Winds on 8 June were light and variable, but were more sustained from the southeast on 10 June. P1 and P2 denote the separate plume interceptions on 10 June described by ref 3. The ordinate and abscissa denote degrees latitude and longitude, respectively.

## METHODOLOGY

The observational data were obtained on two survey flights conducted near the site of the DWH oil platform ( $28^{\circ}44'12''\text{N}$ ,  $88^{\circ}23'13''\text{W}$ ) on 8 and 10 June 2010. Data were filtered to include only those sampled within the lower portion of the marine boundary layer at between 50 and 150 m altitude above sea level. Intermittent periods with elevated CO mixing ratios (>150 ppbv), indicative of combustion sources, were rarely observed but were also excluded from the data set in order to focus solely on the SOA signature. This filtering process also excludes the interception of the plume from a surface oil burn southwest of the DWH site on 8 June.<sup>7</sup> Flight tracks near the DWH site are shown in Figure 1, while the entire, unfiltered flight tracks are provided in the Supporting Information, SI.

**CCN and Aerosol Measurements.** CCN concentration measurements were obtained using a Droplet Measurement Technologies (DMT) stream-wise thermal-gradient cloud condensation nuclei counter (CCNC),<sup>9,10</sup> which exposes an aerosol to a specified water vapor supersaturation and counts and sizes the droplets that form. Since the supersaturation in the instrument is sensitive to pressure fluctuations, the pressure inside the growth chamber was kept constant at 500 hPa using a flow orifice and active control system. On 8 June, the CCNC was operated at a constant flow rate ( $0.5 \text{ L min}^{-1}$ ) and a single supersaturation of 0.33% for the duration of the flight, while on 10 June, the CCNC supersaturation was dynamically scanned over a range of supersaturations (0.2–0.7%) every 15 s using Scanning Flow CCN Analysis (SFCA).<sup>11</sup> Supersaturations were calibrated in terms of the CCNC internal temperature gradient and flow rate using size-classified ammonium sulfate aerosol and Köhler theory.<sup>12–14</sup> The supersaturation absolute uncertainty is estimated to be  $\pm 0.04\%$ .

Subsaturated hygroscopicity measurements were obtained from a cavity ringdown (CRD) spectrometer measuring aerosol extinction at 532 nm wavelength under both dry (10%RH) and humidified (70–95%RH) conditions.<sup>15</sup> Gas phase absorption at 532 nm wavelength was measured using a designated filtered

CRD channel and subtracted from the aerosol measurements but was observed to be low during both flights.

Fine mode dry particle size distribution measurements (0.004 to  $1 \mu\text{m}$  diameter) were obtained every second from an ultrahigh sensitivity aerosol size spectrometer (UHSAS) and a nucleation mode aerosol size spectrometer (NMASS). The NMASS consists of five condensation particle counters (0.004, 0.008, 0.015, 0.030, and  $0.055 \mu\text{m}$  cutoff diameters) that are coupled to the UHSAS distribution using a nonlinear inversion algorithm to obtain the complete size distribution.<sup>16,17</sup>

Nonrefractory, submicrometer aerosol chemical composition was measured using a compact time-of-flight aerosol mass spectrometer (C-ToF-AMS) with a pressure-controlled inlet.<sup>18,19</sup> The instrument was operated in “mass spectrum” mode to obtain bulk (i.e., size-averaged) mass spectra with a 0.1 Hz resolution and in “time-of-flight” mode to obtain size-resolved mass spectra, which were then averaged over 5 min periods to improve the signal-to-noise ratio. The mass spectra were integrated to calculate the total mass loadings for sulfate, nitrate, ammonium, and organic aerosol components. The C-ToF-AMS collection efficiency (CE) parametrization of Middlebrook et al.<sup>20</sup> was used in the data inversion, resulting in an average CE for the flights of  $\sim 0.46$  and  $0.48$ . Mass loadings of elemental carbon were obtained from a single particle soot photometer (SP2) and were found to be much smaller than the nonrefractory mass measured by the C-ToF-AMS.<sup>7,21</sup> Comparison of the total aerosol mass measured by the C-ToF-AMS and SP2 with that derived from the measured size distribution, shows reasonable agreement (slope = 1.11–1.18,  $R^2 = 0.91$ –0.93), verifying the applicability of the chosen C-ToF-AMS CE.

**Coupled CCNC Instrument Model.** An important feature of the DMT CCNC is the ability to measure the size distribution of activated droplets leaving the instrument flow chamber; this makes it possible to retrieve information about CCN activation kinetics. To first order, this can be done by qualitatively comparing the measured droplet size distribution

to that obtained for calibration aerosol (e.g.,  $(\text{NH}_4)_2\text{SO}_4$  or NaCl) at the same instrument operating conditions (flow rate, pressure, and applied temperature gradient). If the measured mean droplet size exceeds that for calibration aerosol, then slow activation kinetics can be ruled out, while a lower measured mean droplet size may suggest slow kinetics. Termed Threshold Droplet Growth Analysis, this procedure has been applied in a number of past studies with success.<sup>22</sup> However, in addition to the basic instrument operating parameters, droplet sizes are also dependent on the aerosol size distribution, and to a lesser extent, the aerosol number concentration in the growth chamber.<sup>22</sup> We use a detailed numerical model to deconvolve these dependencies, allowing the quantification of composition impacts on droplet activation kinetics in terms of an empirical water uptake coefficient,  $\gamma_{\text{cond}}$ , that accounts for gas- and particle-phase mass transfer resistances, solute dissolution kinetics, and for the sticking probability of a water vapor molecule colliding with a growing water droplet.

The coupled CCNC instrument and droplet growth model,<sup>10,22</sup> together with recent improvements by Raatikainen et al.<sup>23</sup> is used here to numerically solve the coupled momentum, mass, and energy balance equations for an aerosol population traversing the CCNC flow field. Model predictions of both the droplet number concentration and size distribution leaving the CCNC growth chamber are compared to the measurements in order to determine the value of  $\gamma_{\text{cond}}$  that gives the best agreement between predicted and measured droplet sizes.

**Analysis.** The ability of a particle to act as a CCN depends on its size, chemical composition, and on the ambient water vapor supersaturation.<sup>12</sup> This compositional dependence is commonly parametrized in terms of a hygroscopicity parameter,  $\kappa$ , in Köhler theory<sup>24</sup>

$$\kappa = \frac{4}{s^2 D_{p,c}^3} \left( \frac{4\sigma M_w}{3RT\rho_w} \right)^3 \quad (1)$$

where  $s$  is the water vapor supersaturation,  $D_{p,c}$  is the particle critical dry diameter (above which all particles act as CCN),  $\sigma$  is the surface tension of the solution droplet,  $R$  is the gas constant,  $T$  is the absolute temperature, and  $M_w$  and  $\rho_w$  are the molar mass and density of water, respectively. In this study, the surface tension of pure water ( $71.4 \text{ mJ m}^{-2}$ ) is assumed. Following Moore et al.<sup>25</sup> and as described in the SI,  $\kappa$  is calculated by integrating the aerosol size distribution above some  $D_{p,c}$  so that the integrated concentration matches the measured CCN concentration at a specified supersaturation. This value of  $D_{p,c}$  is then used in eq 1 to find  $\kappa$ . Given the range of supersaturations and observed  $D_{p,c}$ , a more complex form of eq 1 is not necessary.

While the hygroscopicity parameter is unable to unambiguously account for complex aerosol mixing state or surface tension impacts, using the above approach offers a simple way to parametrize composition for global models and is applicable to other measures of water uptake, such as in subsaturated conditions. While  $\kappa$  is expected to be similar for both water vapor saturation ratios less than and greater than unity, solution nonideality or surface tension effects in the former may yield a derived subsaturated  $\kappa$  that is somewhat lower than for supersaturated cloud droplets, which are more dilute.<sup>24,26,27</sup>

The subsaturated humidity dependence of the CRD aerosol extinction was used to derive the aerosol humidification factor,  $\gamma_{\text{ext}}$ , as follows:

$$\frac{\sigma_{\text{RH}}}{\sigma_{\text{RH}_{\text{ref}}}^{\text{ext}}} = \left[ \frac{1 - \text{RH}}{1 - \text{RH}_{\text{ref}}} \right]^{\gamma_{\text{ext}}} \quad (2)$$

where  $\sigma_{\text{RH}}$  is the measured aerosol extinction at relative humidity, RH. In this work, the reference RH is 10%, while the elevated RH is 85%. The humidification factor represents the dependence of aerosol extinction on RH, which results from changes in the particle size and refractive index upon humidification. Thus,  $\gamma_{\text{ext}}$  and  $\kappa$  are related quantities and one can employ Mie theory with a number of assumptions to independently derive  $\kappa$  from  $\gamma_{\text{ext}}$ . These calculations were performed using the CRD data together with the measured dry particle size distribution and a prescribed refractive index (RI) of  $1.45 - 0i$ . Further details regarding the calculation approach and sensitivity to the RI assumption and  $\sigma$  uncertainty are presented in the SI.

## RESULTS AND DISCUSSION

**CCN Activity and Hygroscopicity.** Figure 1 shows the collocated spatial distribution of the CCN-derived  $\kappa$  and the organic aerosol volume fraction for the low-level flight legs near the DWH site. Greater variability in  $\kappa$  for adjacent points far from the DWH site on 10 June exceeds that seen on 8 June, which may reflect size-dependent aerosol composition because the changing instrument supersaturation during SFCA operation on 10 June also changes the size range over which CCN measurements are most sensitive (i.e., diameters near  $D_{p,c}$ ). Winds on 8 June were light with variable direction, while a more sustained southeasterly flow was present on 10 June. This gives rise to a distinct plume of low-hygroscopicity, organic aerosol to the northwest of the DWH site on the 10th. deGouw et al.<sup>3</sup> examined the gas- and aerosol-phase composition on this day for a plume transect near the DWH site (P1) and a transect farther downwind (P2). They found a narrow plume of VOCs surrounded by a much broader plume of hydrocarbon-like SOA, with the organic aerosol concentration and size distribution both increasing from P1 to P2.<sup>3</sup> Transport calculations based on wind speed and direction suggest that the enhancement in SOA results from less-volatile IVOC precursors (likely  $C_{14}$  to  $C_{16}$  compounds), which evaporate over a period of hours to days after surfacing and are chemically transformed to SOA within a few hours in the atmosphere.<sup>3</sup> The importance of a sustained wind direction in dispersing the oil emissions is apparent from the lack of an appreciable organic fraction south of the DWH site on the 10th, but a wider impacted area on the 8th. Satellite imagery of the spill extent (gray shaded region in Figure 1) on both days does not necessarily coincide with enhancements in gas- or aerosol-phase species, suggesting that the “highly-aged” portion of the oil slick consists of low volatility compounds, which do not contribute appreciably to SOA.

The changes in the total particle size distribution ( $dN_{\text{CN}}/d\log D_p$ ) and CCN supersaturation distribution ( $dN_{\text{CCN}}/ds$ ) across different organic aerosol fractions are shown in Figure 2. The solid trace denotes the geometric means and the circles denote the mean values for P1 and P2. A small accumulation mode of a few thousand particles per  $\text{cm}^3$  is present at all organic fractions with a significant Aitken mode appearing at

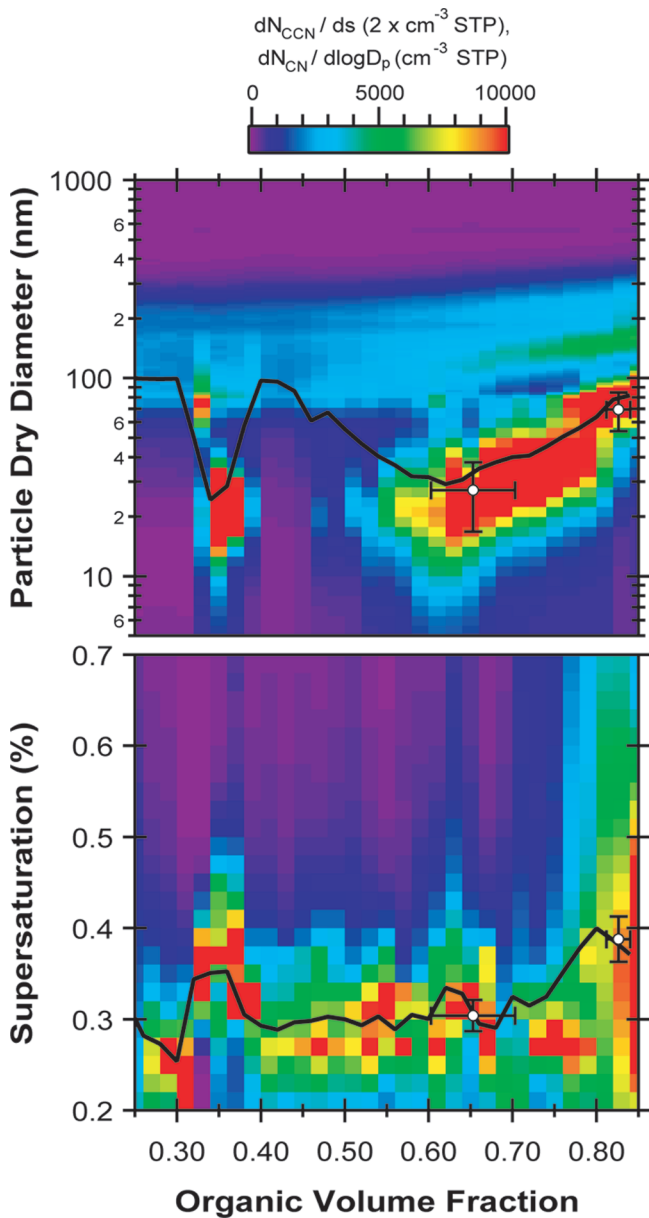


**Figure 2.** Average particle size distributions (top) and CCN supersaturation distributions (bottom) plotted versus the C-ToF-AMS organic volume fraction for the 10 June flight. Solid traces denote the geometric mean diameter and supersaturation in the top and bottom figures, respectively, calculated for a single mode. Circles show the mean values for the intercepted plume at P1 and P2 ( $\pm 1$  standard deviation).

organic fractions above 60%. The mean size of the Aitken mode increases by roughly 3-fold over the observed range of organic fractions, consistent with condensational growth from semi-volatile organic vapors. A large Aitken mode is also present in Figure 2 between 30–40% organics, which reflects the sampling of freshly nucleated particles in the absence of organic condensation on existing large particles just upwind of the DWH site.<sup>28</sup> For organic volume fractions less than 75–80%, the peak of the CCN distribution is around  $(0.30 \pm 0.05)\%$  supersaturation, which broadens considerably and shifts to approximately  $(0.4 \pm 0.1)\%$  supersaturation at the highest organic fractions.

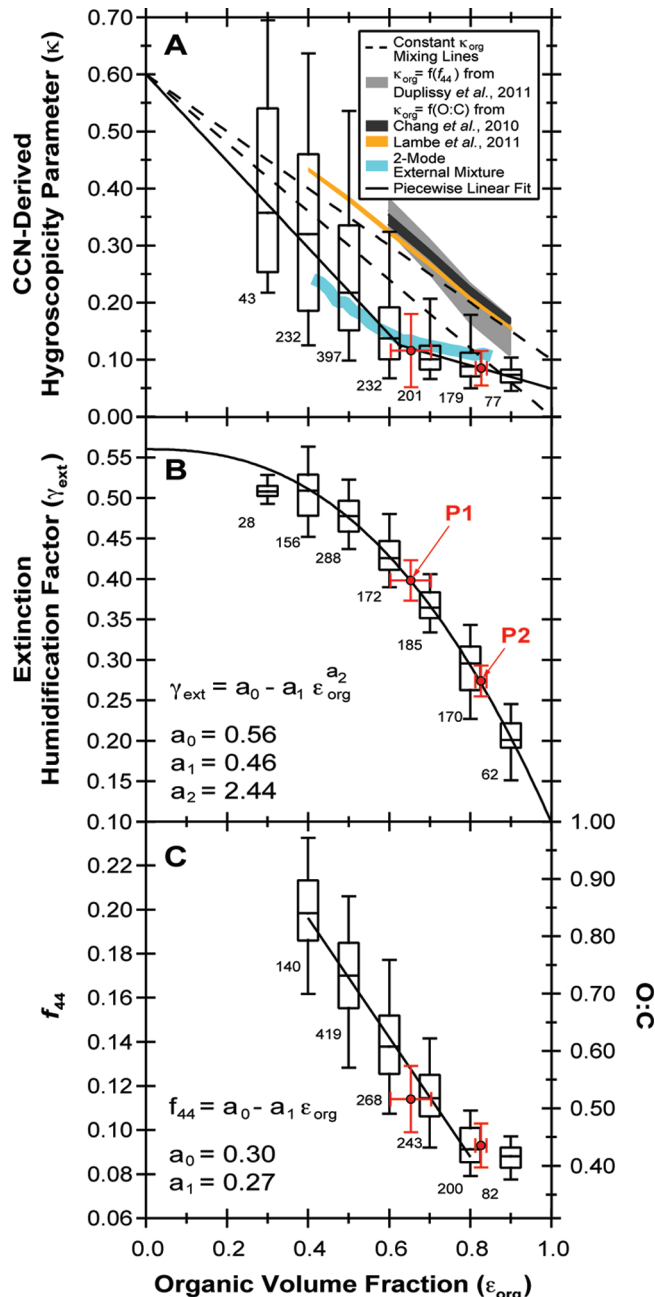


**Figure 3.** Distribution of (a) CCN-derived hygroscopicity, (b) extinction humification factor, and (c)  $f_{44}$  ratio and O:C ratio (from the Aiken et al.<sup>33</sup> correlation) plotted versus C-ToF-AMS organic volume fraction. Boxes denote the median and interquartile range for all observations from both flights between 50 and 150 m altitude, while the numbers beside each box denote the number of 0.1 Hz points used in the calculation. Solid traces are fits to the median data. Circles show the mean values for the intercepted plume at P1 and P2 on June 10th ( $\pm 1$  standard deviation). Shaded areas and dashed traces in (a) are  $\kappa$  predictions from different compositional assumptions. The organic volume fraction bin centered at 0.25 in (c) has been excluded due to a low signal-to-noise ratio.

The increase in critical supersaturation coincides with an increase in the mean particle diameter, which implies a significant decrease in the particle hygroscopicity since increasing particle size tends to strongly decrease the critical supersaturation. This is shown by the inverse correlation between  $\kappa$ ,  $\gamma_{ext}$ , and organic volume fraction in Figure 3a,b. The

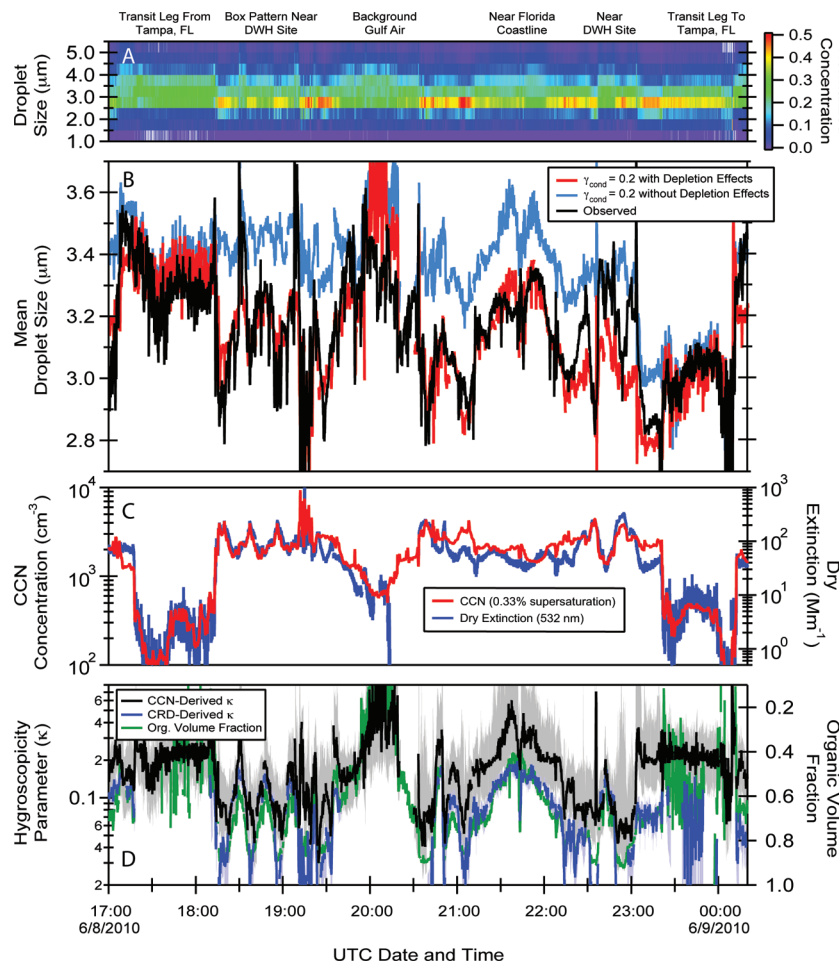


**Figure 4.** Timeseries of measured (a, b) and modeled (b) droplet sizes of activated CCN in the CCNC during the June eighth flight. Shown for comparison are the measured CCN concentrations and dry extinction at 532 nm (c) and the aerosol organic volume fraction and hygroscopicities derived from the supersaturated CCN and subsaturated cavity ring down measurements (d). The shaded regions in (d) denote the propagated uncertainty of each  $\kappa$  ( $\pm 1$  standard deviation), whose calculation is described in the SI.

overall  $\kappa$  for an aerosol containing  $n$  components is calculated as follows:

$$\kappa = \sum_i^n \varepsilon_i \kappa_i \quad (3)$$

where  $\varepsilon_i$  and  $\kappa_i$  are the volume fraction and hygroscopicity of the  $i$ -th aerosol component, respectively. Two-component mixing lines were calculated from eq 3 assuming a constant inorganic hygroscopicity,  $\kappa_{\text{inorg}}$ , of 0.6 and a constant organic hygroscopicity,  $\kappa_{\text{org}}$ , of either 0 or 0.1 (dashed traces in Figure 3a). It can be seen from Figure 3a that the observed aerosol hygroscopicity lies below even the  $\kappa_{\text{org}} = 0$  mixing line, which likely reflects size-dependent composition or a partially externally mixed aerosol population not captured by these simple, but commonly employed, mixing rules. Extrapolating the piecewise linear fit of the median  $\kappa$  data in Figure 3a to  $\varepsilon_{\text{org}} = 1$  yields an effective  $\kappa_{\text{org}} = 0.05$ . In modeling the condensational growth rate of SOA near the DWH site, Brock et al.<sup>28</sup> assumed an intermediate-volatility organic species with a molar mass of  $0.292 \text{ kg mol}^{-1}$  and density of  $1000 \text{ kg m}^{-3}$ . From Köhler theory, the hygroscopicity of a pure, soluble organic aerosol can be found as  $\kappa_{\text{org}} = (M_w/\rho_w)(\rho_{\text{org}}/M_{\text{org}})\nu_{\text{org}}$  where  $\rho_{\text{org}}$ ,  $M_{\text{org}}$ , and  $\nu_{\text{org}}$  are the density, molar mass, and van't Hoff factor of the organic solute,<sup>36</sup> Using the

values of  $\rho_{\text{org}}$  and  $M_{\text{org}}$  from Brock et al.<sup>28</sup> with an assumed unit van't Hoff factor yields a value of 0.06, which is consistent with the CCN-derived estimate.

A number of ambient and SOA chamber studies have shown that the pure organic hygroscopicity increases with increasing organic oxygenation.<sup>29–32</sup> The C-ToF-AMS mass fraction of the  $m/z$  44 peak to total organic mass,  $f_{44}$ , is correlated with the organic O:C ratio,<sup>33,34</sup> and the relationship between  $\kappa_{\text{org}}$  and  $f_{44}$  or O:C has been reported for some previous measurements.<sup>30–32</sup> From Figure 3c, it can be observed that aerosol composed almost entirely of SOA are less oxidized than aerosol composed only partially of SOA. This trend reflects the varying contribution of the low-O:C, fresh SOA and the higher-O:C, aged background organic aerosol to the total aerosol composition, where the former dominate at high  $\varepsilon_{\text{org}}$  near the DWH site and the latter dominate at lower  $\varepsilon_{\text{org}}$  outside of these SOA plumes. Using three parametrizations for  $\kappa_{\text{org}}$  and a constant  $\kappa_{\text{inorg}} = 0.6$  yields the shaded regions shown in Figure 3a, which considerably overpredict the aerosol hygroscopicity parameter by a similar amount as the  $\kappa_{\text{org}} = 0.1$  mixing line.

As shown in Figure 2, a distinct accumulation size mode is present throughout the survey flights with a more prominent Aitken size mode associated with the organic-rich aerosol near the DWH site. Consequently, size-resolved C-ToF-AMS chemical composition was used to look for compositional

differences between the two modes, which may explain the overprediction shown in Figure 3a. As discussed in the SI, a lower size-resolved, organic volume fraction  $\varepsilon_{\text{SR,org}}$  was observed for the accumulation mode ( $\sim 0.4\text{--}0.8$ ) versus the Aitken mode ( $\sim 0.85\text{--}1$ ). While the larger-sized particles affect the bulk (i.e., size-averaged) C-ToF-AMS composition more so than the smaller particles, the Aitken-mode-dominated number size distribution is a more important determinant of CCN activity. Using the average composition for each mode,  $\kappa$  was calculated for both the accumulation mode and the Aitken mode aerosol assuming  $\kappa_{\text{org}} = 0.05$  and  $\kappa_{\text{inorg}} = 0.6$ . The overall  $\kappa$  is then obtained from a CCN number-weighted average of the two modes and is shown as the blue shaded region in Figure 3, where it can be seen that predictions of  $\kappa$  based on a two-mode, size-dependent composition are in much better agreement with observations than those obtained from bulk (i.e., size-averaged) composition, both using the same simple mixing rule assumptions.

A comparison between the supersaturated, CCN-derived  $\kappa_{\text{CCN}}$  and the subsaturated, CRD-derived  $\kappa_{\text{CRD}}$  is shown for the entire June 8 flight in Figure 4d. For most of the flight, the mean value of  $\kappa_{\text{CRD}}$  is approximately 50% less than  $\kappa_{\text{CCN}}$  (Figure S3 of the SI), although the data are highly correlated assuming a constant 50% bias ( $R^2 = 0.75$ ) and the propagated uncertainty of  $\kappa_{\text{CCN}}$  is relatively large. A similar discrepancy ( $\sim 30\text{--}50\%$ ) has been previously observed for comparison of CCN-derived hygroscopicities and those inferred from subsaturated measurements with an humidified tandem differential mobility analyzer (HTDMA).<sup>26,27,35</sup> This suggests that while the humidification of organic-rich aerosol appears to have a small effect on their size and light scattering ( $\kappa_{\text{CRD}} \approx 0.01\text{--}0.05$ ), these particles have a greater contribution to CCN activation ( $\kappa_{\text{CCN}} \approx 0.05\text{--}0.10$ ).

The derived organic hygroscopicity of  $\sim 0.05$  is on the low end of past studies looking at the CCN-derived  $\kappa$  of SOA produced from the oxidation of IVOCs, but is consistent with some past subsaturated hygroscopic growth results. For example, Jimenez et al.<sup>29</sup> report  $\kappa_{\text{org}} \approx 0.06$  from hygroscopic growth measurements of aerosol in Mexico City and from the smog chamber oxidation of  $\alpha$ -pinene for aerosol with O:C  $\approx 0.4$ . Meanwhile, CCN measurements have found  $\kappa_{\text{org}}$  of 0.04 for  $\beta$ -caryophyllene SOA produced via ozonolysis,<sup>36</sup> of 0.01–0.10 for SOA derived from the OH oxidation of *n*-heptadecane (O:C  $\approx 0.1\text{--}0.2$ ),<sup>32</sup> and of 0.07–0.10 for SOA derived from the OH oxidation of longifolene (O:C  $\approx 0.2\text{--}0.3$ ). This work is contrasted with many other studies of ambient SOA in the literature that find higher  $\kappa$  on the order of 0.1–0.3,<sup>37–41</sup> likely due to the more-aged nature of the sampled aerosol, which increases both  $\kappa$  and O:C. Thus, this work provides important observations of the CCN-derived hygroscopicity of relatively unoxidized SOA derived from IVOCs that likely require less oxidation in the atmosphere to form reaction products which partition into the aerosol phase.<sup>42,43</sup> Near local emissions sources such as in urban environments, the presence of these less hygroscopic SOA species may partially explain some large CCN overpredictions based on measured aerosol composition.<sup>44</sup>

**Droplet Activation Kinetics.** Figure 4a,b presents the droplet size distribution of activated CCN in the CCNC (normalized by the total number of droplets), the number-averaged mean droplet size, and the modeled mean droplet size for aerosol with an effective water uptake coefficient,  $\gamma_{\text{cond}}$ , of 0.2. It can be seen that the temporal variability is strongly

correlated for the measured and modeled mean droplet sizes when accounting for supersaturation depletion effects from moderate CCN concentrations in the CCNC growth chamber ( $\sim 1000\text{--}3000 \text{ cm}^{-3}$  STP).<sup>22</sup> Neglecting the depletion effects leads to a larger mean droplet size and much less variability in the predictions, which is not in agreement with observations. This is because, even though supersaturation depletion has a limited effect on the measured CCN concentration, it can have an observable effect on the measured droplet size distribution. The simulated traces were corrected by a constant  $2.3 \mu\text{m}$  bias, which gives the best agreement between the  $\gamma_{\text{cond}} = 0.2$  simulated and observed droplet sizes (see SI). Simulations of the activation and growth of ammonium sulfate calibration aerosol reveal a  $2.1 \mu\text{m}$  model overprediction bias, which is in good agreement with the correction bias applied here. Regression analysis of the modeled versus measured mean droplet sizes indicates that a constant value of  $\gamma_{\text{cond}}$  between 0.1 and 0.2 best reproduces the observed droplet size variability for the entire data set.

While it is known that droplet formation is less sensitive to changes in  $\gamma_{\text{cond}}$  in the range of 0.1–1 versus lower values,<sup>45</sup> the exact value of  $\gamma_{\text{cond}}$ , even for pure water droplets, remains uncertain with reported values in the range from 0.04 to 1.<sup>46–49</sup> The most realistic value is probably between 0.06 and 0.3.<sup>47,48,50</sup> As the inferred coefficients in this study are similar to the reference values for pure water, this suggests that the fresh SOA generated near the DWH site do not promote kinetic delays upon condensation on ambient CCN. Given the relatively low hygroscopicity and hydrocarbon-like nature of the organic species (O:C ratios  $\sim 0.4\text{--}0.5$  around the plume), this is a somewhat unexpected result. Previous work has shown that hydrophobic organic compounds may retard water uptake through slow dissolution, which reduces the amount of solute in the droplet and shifts the water vapor–liquid equilibrium more toward the gas-phase than if all of the solute had immediately dissolved.<sup>51</sup> Alternatively, organics may form compressed films on the droplet surface, which increases the condensational mass transfer resistance.<sup>52</sup> A number of past studies have found distinctly slower activation kinetics for smog-chamber SOA resulting from the photo-oxidation of  $\beta$ -caryophyllene,<sup>53</sup> aerosol above the Pacific marine boundary layer,<sup>54</sup> biogenic aerosol in rural Canada,<sup>55</sup> and both urban and rural aerosol at ground-based locations around the United States.<sup>56</sup> Lance et al.<sup>57</sup> examined airborne measurements of CCN in Houston, TX, during the 2006 GoMACCS campaign and found no evidence for slow activation kinetics,<sup>57</sup> contrary to Ruehl et al.<sup>54</sup> and AsaAwuku et al.,<sup>58</sup> who did observe delayed CCN activation from concurrent ground-based and airborne platforms. Since some of these studies were carried out with size-selected aerosol (i.e., a small fraction of the overall CCN concentration was sampled at a time), supersaturation depletion effects may not have caused the apparent kinetic delays. A potential difference may be the phase state of the aerosol (e.g., glassy/amorphous versus partially deliquesced) and its impact on water uptake kinetics. Given that most kinetic delays were reported for dry aerosol may lend some support to this hypothesis. A previously deliquesced aerosol state is consistent with the current results as even a small amount of residual water could inhibit glassy transition and promote rapid activation kinetics. If true, then this suggests that condensation of even the most hydrophobic SOA onto existing inorganic CCN may not impact activation kinetics. This finding is relevant for the growth of newly formed particles in the

atmosphere, which have been hypothesized to form as  $\text{H}_2\text{SO}_4$  seeds and grow to CCN-relevant sizes primarily through the condensation of SOA from IVOCs and VOCs.<sup>59–61</sup>

## ■ ASSOCIATED CONTENT

### Supporting Information

Analysis methods and calculations, results and discussion, and additional figures. This material is available free of charge via the Internet at <http://pubs.acs.org/>.

## ■ AUTHOR INFORMATION

### Corresponding Author

\*E-mail: athanasiос.nenes@gatech.edu.

### Notes

The authors declare no competing financial interest.

## ■ ACKNOWLEDGMENTS

R.H.M. acknowledges support from DOE GCEP and NASA ESS Graduate Research Fellowships. T.R. acknowledges support from the Finnish Cultural Foundation. A.N. and R.H.M. acknowledge support from NOAA and NSF CAREER. We acknowledge K. Cerully for CCN support during the California component of CalNex, and thank T. Ryerson and J. de Gouw for helpful comments on this manuscript.

## ■ REFERENCES

- (1) Crone, T. J.; Tolstoy, M. Magnitude of the 2010 Gulf of Mexico oil leak. *Science* **2010**, *330*, 634.
- (2) Ryerson, T. B.; et al. Atmospheric emissions from the Deepwater Horizon spill constrain air water partitioning, hydrocarbon fate, and leak rate. *Geophys. Res. Lett.* **2011**, *38*.
- (3) de Gouw, J. A.; et al. Organic aerosol formation downwind from the Deepwater Horizon oil spill. *Science* **2011**, *331*, 1295–1299.
- (4) de Gouw, J.; Jimenez, J. L. Organic aerosols in the earth's atmosphere. *Environ. Sci. Technol.* **2009**, *43*, 7614–7618.
- (5) Hallquist, M.; et al. The formation, properties and impact of secondary organic aerosol: Current and emerging issues. *Atmos. Chem. Phys.* **2009**, *9*, 5155–5236.
- (6) Zhang, Q.; et al. Ubiquity and dominance of oxygenated species in organic aerosols in anthropogenically-influenced Northern Hemisphere midlatitudes. *Geophys. Res. Lett.* **2007**, *34*.
- (7) Perring, A. E.; Schwarz, J. P.; Spackman, J. R.; Bahreini, R.; de Gouw, J. A.; Gao, R. S.; Holloway, J. S.; Lack, D. A.; Langridge, J. M.; Peischl, J.; Middlebrook, A. M.; Ryerson, T. B.; Warneke, C.; Watts, L. A.; Fahey, D. W. Characteristics of black carbon aerosol from a surface oil burn during the Deepwater Horizon Oil spill. *Geophys. Res. Lett.* **2011**, *38*.
- (8) NOAA-NESDIS, Satellite Derived Surface Oil Analysis Products – Deepwater Horizon ([www.ssd.noaa.gov/PS/MPS/deepwater.html](http://www.ssd.noaa.gov/PS/MPS/deepwater.html)). 2010.
- (9) Roberts, G. C.; Nenes, A. A continuous-flow streamwise thermal-gradient CCN chamber for atmospheric measurements. *Aerosol Sci. Technol.* **2005**, *39*, 206–221.
- (10) Lance, S.; Medina, J.; Smith, J. N.; Nenes, A. Mapping the operation of the DMT continuous flow CCN counter. *Aerosol Sci. Technol.* **2006**, *40*, 242–254.
- (11) Moore, R. H.; Nenes, A. Scanning flow CCN analysis—A method for fast measurements of CCN spectra. *Aerosol Sci. Technol.* **2009**, *43*, 1192–1207.
- (12) Köhler, H. The nucleus in and growth of hygroscopic droplets. *Trans. Faraday Soc.* **1936**, *32*, 1152–1161.
- (13) Rose, D.; Gunthe, S. S.; Mikhailov, E.; Frank, G. P.; Dusek, U.; Andreae, M. O.; Pöschl, U. Calibration and measurement uncertainties of a continuous-flow cloud condensation nuclei counter (DMT-CCNC): CCN activation of ammonium sulfate and sodium chloride aerosol particles in theory and experiment. *Atmos. Chem. Phys.* **2008**, *8*, 1153–1179.
- (14) Moore, R. H.; Nenes, A.; Medina, J. Scanning mobility CCN analysis—A method for fast measurements of size-resolved CCN distributions and activation kinetics. *Aerosol Sci. Technol.* **2010**, *44*, 861–871.
- (15) Langridge, J. M.; Richardson, M. S.; Lack, D.; Law, D.; Murphy, D. M. Aircraft instrumentation for comprehensive characterization of aerosol optical properties, Part I: Wavelength dependent optical extinction and its relative humidity dependence measured using cavity ring down spectroscopy. *Aerosol Sci. Technol.* **2011**, *45*, 1305–1318.
- (16) Brock, C. A.; Schröder, F.; Kärcher, B.; Petzold, A.; Busen, R.; Fiebig, M. Ultrafine particle size distributions measured in aircraft exhaust plumes. *J. Geophys. Res.* **2000**, *105*, 26,555–26,567.
- (17) Brock, C. A.; et al. Characteristics, sources, and transport of aerosols measured in Spring 2008 during the Aerosol, Radiation, and Cloud Processes Affecting Arctic Climate (ARCPAC) project. *Atmos. Chem. Phys.* **2011**, *11*, 2423–2453.
- (18) Bahreini, R.; Dunlea, E. J.; Matthew, B. M.; Simons, C.; Docherty, K. S.; DeCarlo, P. F.; Jimenez, J. L.; Brock, C. A.; Middlebrook, A. M. Design and operation of a pressure controlled inlet for airborne sampling with an aerodynamic aerosol lens. *Aerosol Sci. Technol.* **2008**, *42*, 465–471.
- (19) Drewnick, F.; Hings, S. S.; DeCarlo, P.; Jayne, J. T.; Gonin, M.; Fuhrer, K.; Weimer, S.; Jimenez, J. L.; Demerjian, K. L.; Borrmann, S.; Worsnop, D. R. A new time-of-flight aerosol mass spectrometer (TOF-AMS) – Instrument description and first field deployment. *Aerosol Sci. Technol.* **2005**, *39*, 637–658.
- (20) Middlebrook, A. M.; Bahreini, R.; Jimenez, J. L.; Canagaratna, M. R. Evaluation of composition-dependent collection efficiencies for the Aerodyne aerosol mass spectrometer using field data. *Aerosol Sci. Technol.* **2012**, *46*, 258–271.
- (21) Schwarz, J. P.; Spackman, J. R.; Fahey, D. W.; Gao, R. S.; Lohmann, U.; Stier, P.; Watts, L. A.; Thomson, D. S.; Lack, D. A.; Pfister, L.; Mahoney, M. J.; Baumgardner, D.; Wilson, J.; Reeves, J. M. Coatings and their enhancement of black carbon light absorption in the tropical atmosphere. *J. Geophys. Res.* **2008**, *113*.
- (22) Lathem, T.; Nenes, A. Water vapor depletion in the DMT continuous flow CCN chamber: Effects on supersaturation and droplet growth. *Aerosol Sci. Technol.* **2011**, *45*, 604–615.
- (23) Raatikainen, T.; Moore, R. H.; Lathem, T. L.; Nenes, A. A coupled observation—Modeling approach for studying activation kinetics from measurements of CCN activity. *Atmos. Chem. Phys. Discuss.* **2012**, *12*, 1821–1865.
- (24) Petters, M. D.; Kreidenweis, S. M. A single parameter representation of hygroscopic growth and cloud condensation nucleus activity. *Atmos. Chem. Phys.* **2007**, *7*, 1961–1971.
- (25) Moore, R. H.; Bahreini, R.; Brock, C. A.; Froyd, K. D.; Cozic, J.; Holloway, J. S.; Middlebrook, A. M.; Murphy, D. M.; Nenes, A. Hygroscopicity and composition of Alaskan Arctic CCN during April 2008. *Atmos. Chem. Phys.* **2011**, *11*, 11807–11825.
- (26) Massoli, P.; et al. Relationship between aerosol oxidation level and hygroscopic properties of laboratory generated secondary organic aerosol (SOA) particles. *Geophys. Res. Lett.* **2010**, *37*.
- (27) Cerully, K. M.; Raatikainen, T.; Lance, S.; Tkacik, D.; Tiitta, P.; Petäjä, T.; Ehni, M.; Kulmala, M.; Worsnop, D. R.; Laaksonen, A.; Smith, J. N.; Nenes, A. Aerosol hygroscopicity and CCN activation kinetics in a boreal forest environment during the 2007 EUCAARI campaign. *Atmos. Chem. Phys.* **2011**, *11*, 15029–15074.
- (28) Brock, C. A.; Murphy, D. M.; Bahreini, R.; Middlebrook, A. M. Formation and growth of organic aerosols downwind of the Deepwater Horizon oil spill. *Geophys. Res. Lett.* **2011**, *38*.
- (29) Jimenez, J.; et al. Evolution of organic aerosols in the atmosphere. *Science* **2009**, *326*, 1525–1529.
- (30) Chang, R. Y.-W.; Slowik, J. G.; Shantz, N. C.; Vlasenko, A.; Liggio, J.; Sjostedt, S. J.; Leaitch, W. R.; Abbatt, J. P. D. The hygroscopicity parameter ( $k$ ) of ambient organic aerosol at a field site subject to biogenic and anthropogenic influences: Relationship to degree of aerosol oxidation. *Atmos. Chem. Phys.* **2010**, *10*, 5047–5064.

- (31) Duplissy, J.; et al. Relating hygroscopicity and composition of organic aerosol particulate matter. *Atmos. Chem. Phys.* **2011**, *11*, 1155–1165.
- (32) Lambe, A. T.; Onasch, T. B.; Massoli, P.; Croasdale, D. R.; Wright, J. P.; Ahern, A. T.; Williams, L. R.; Worsnop, D. R.; Brune, W. H.; Davidovits, P. Laboratory studies of the chemical composition and cloud condensation nuclei (CCN) activity of secondary organic aerosol (SOA) and oxidized primary organic aerosol (OPOA). *Atmos. Chem. Phys.* **2011**, *11*, 8913–8928.
- (33) Aiken, A. C.; et al. O/C and OM/OC ratios of primary, secondary, and ambient organic aerosols with high-resolution time-of-flight aerosol mass spectrometry. *Environ. Sci. Technol.* **2008**, *42*, 4478–4485.
- (34) Zhang, Q.; Alfara, M. R.; Worsnop, D. R.; Allan, J. D.; Coe, H.; Canagaratna, M. R.; Jimenez, J. L. Deconvolution and quantification of hydrocarbon-like and oxygenated organic aerosols based on aerosol mass spectrometry. *Environ. Sci. Technol.* **2005**, *39*, 4938–4952.
- (35) Roberts, G. C.; Day, D. A.; Russell, L. M.; Dunlea, E. J.; Jimenez, J. L.; Tomlinson, J. M.; Collins, D. R.; Sinozuka, Y.; Clark, A. D. Characterization of particle cloud droplet activity and composition in the free troposphere and the boundary layer during INTEX-B. *Atmos. Chem. Phys.* **2010**, *10*, 6627–6644.
- (36) Asa-Awuku, A.; Nenes, A.; Gao, S.; Flagan, R. C.; Seinfeld, J. H. Water-soluble SOA from alkene ozonolysis: Composition and droplet activation kinetics inferences from analysis of CCN activity. *Atmos. Chem. Phys.* **2010**, *10*, 1585–1597.
- (37) Engelhart, G. J.; Moore, R. H.; Nenes, A.; Pandis, S. N. Cloud condensation nuclei activity of isoprene secondary organic aerosol. *J. Geophys. Res.* **2011**, *116*.
- (38) Dusek, U.; Frank, G. P.; Curtius, J.; Drewnick, F.; Schneider, J.; Kürten, A.; Rose, D.; Andreae, M. O.; Borrmann, S.; Pöschl, U. Enhanced organic mass fraction and decreased hygroscopicity of cloud condensation nuclei (CCN) during new particle formation events. *Geophys. Res. Lett.* **2010**, *37*.
- (39) Gunthe, S. S.; King, S. M.; Rose, D.; Chen, Q.; Roldin, P.; Farmer, D. K.; Jimenez, J. L.; Andreae, M. O.; Martin, S. T.; Pöschl, U. Cloud condensation nuclei in pristine tropical rainforest air of Amazonia: Size-resolved measurements and modeling of atmospheric aerosol composition and CCN activity. *Atmos. Chem. Phys.* **2009**, *9*, 7551–7575.
- (40) Pringle, K. J.; Tost, H.; Pozzer, A.; Pöschl, U.; Lelieveld, J. Global distribution of the effective aerosol hygroscopicity parameter for CCN activation. *Atmos. Chem. Phys.* **2010**, *10*, 5241–5255.
- (41) Andreae, M. O.; Rosenfeld, D. Aerosol-cloud-precipitation interactions. Part 1. The nature and sources of cloud-active aerosols. *Earth-Sci. Rev.* **2008**, *89*, 13–41.
- (42) Robinson, A. L.; Donahue, N. M.; Shrivastava, M. K.; Weitkamp, E. A.; Sage, A. M.; Grieshop, A. P.; Lane, T. E.; Pierce, J. R.; Pandis, S. N. Rethinking organic aerosols: Semivolatile emissions and photochemical aging. *Science* **2007**, *315*, 1259–1262.
- (43) Presto, A. A.; Miracolo, M. A.; Kroll, J. H.; Worsnop, D. R.; Robinson, A. L.; Donahue, N. M. Intermediate-volatility organic compounds: A potential source of ambient oxidized organic aerosol. *Environ. Sci. Technol.* **2009**, *43*, 4744–4749.
- (44) Ervens, B.; Cubison, M. J.; Andrews, E.; Feingold, G.; Ogren, J. A.; Jimenez, J. L.; Quinn, P. K.; Bates, T. S.; Wang, J.; Zhang, Q.; Coe, H.; Flynn, M.; Allan, J. D. CCN predictions using simplified assumptions of organic aerosol composition and mixing state: A synthesis from six different locations. *Atmos. Chem. Phys.* **2010**, *10*, 4795–4807.
- (45) Nenes, A.; Charlson, R. J.; Facchini, M. C.; Kulmala, M.; Laaksonen, A.; Seinfeld, J. H. Can chemical effects on cloud droplet number rival the first indirect effect? *Geophys. Res. Lett.* **2002**, *29*.
- (46) Davis, E. J. A history and state-of-the-art of accommodation coefficients. *Atmos. Res.* **2006**, *82*, 561–578.
- (47) Li, Y. Q.; Davidovits, P.; Shi, Q.; Jayne, J. T.; Kolb, C. E.; Worsnop, D. R. Mass and thermal accommodation coefficients of  $H_2O(g)$  on liquid water as a function of temperature. *J. Phys. Chem. A* **2001**, *105*, 10627–10634.
- (48) Shaw, R. A.; Lamb, D. Experimental determination of the thermal accommodation and condensation coefficients of water. *J. Chem. Phys.* **1999**, *111*, 10659–106663.
- (49) Mozurkewich, M. Aerosol growth and the condensation coefficient for water: A review. *Aerosol Sci. Technol.* **1986**, *5*, 223–236.
- (50) Fountoukis, C.; Nenes, A.; Meskhidze, N.; Bahreini, R.; Conant, W. C.; Jonsson, H.; Murphy, S.; Sorooshian, A.; Varutbangkul, V.; Brechtel, F.; Flagan, R. C.; Seinfeld, J. H. Aerosol cloud drop concentration closure for clouds sampled during the International Consortium for Atmospheric Research on Transport and Transformation 2004 campaign. *J. Geophys. Res.* **2007**, *112*.
- (51) Asa-Awuku, A.; Nenes, A. The effect of solute dissolution kinetics on cloud droplet formation: Extended Köhler theory. *J. Geophys. Res.* **2007**, *112*.
- (52) Rubel, G. O.; Gentry, J. W. Measurement of the kinetics of solution droplets in the presence of adsorbed monolayers: Determination of water accommodation coefficients. *J. Phys. Chem.* **1984**, *88*, 3142–3148.
- (53) Asa-Awuku, A.; Engelhart, G.; Lee, B.; Pandis, S.; Nenes, A. Relating CCN activity, volatility, and droplet growth kinetics of  $\beta$ -caryophyllene secondary organic aerosol. *Atmos. Chem. Phys.* **2009**, *9*, 795–812.
- (54) Ruehl, C. R.; Chuang, P. Y.; Nenes, A. Distinct CCN activation kinetics above the marine boundary layer along the California coast. *Geophys. Res. Lett.* **2009**, *36*.
- (55) Shantz, N. C.; Chang, R. Y.-W.; Slowik, J. G.; Vlasenko, A.; Abbatt, J. P. D.; Leaitch, W. R. Slower CCN growth kinetics of anthropogenic aerosol compared to biogenic aerosol observed at a rural site. *Atmos. Chem. Phys.* **2010**, *10*, 299–312.
- (56) Ruehl, C. R.; Chuang, P. Y.; Nenes, A. How quickly do cloud droplets form on atmospheric particles? *Atmos. Chem. Phys.* **2008**, *8*, 1043–1055.
- (57) Lance, S.; Nenes, A.; Mazzoleni, C.; Dubey, M. K.; Gates, H.; Varutbangkul, V.; Rissman, T. A.; Murphy, S. M.; Sorooshian, A.; Flagan, R. C.; Seinfeld, J. H.; Feingold, G.; Jonsson, H. H. Cloud condensation nuclei activity, closure, and droplet growth kinetics of Houston aerosol during the Gulf of Mexico Atmospheric Composition and Climate Study (GoMACCS). *J. Geophys. Res.* **2009**, *114*.
- (58) Asa-Awuku, A.; Moore, R. H.; Nenes, A.; Bahreini, R.; Holloway, J. S.; Brock, C. A.; Middlebrook, A. M.; Ryerson, T. B.; Jimenez, J. L.; DeCarlo, P. F.; Hecobian, A.; Weber, R. J.; Stickel, R.; Tanner, D. J.; Huey, L. G. Airborne cloud condensation nuclei measurements during the 2006 Texas Air Quality Study. *J. Geophys. Res.* **2011**, *116*.
- (59) Kulmala, M.; Kerminen, V.-M. On the formation and growth of atmospheric nanoparticles. *Atmos. Res.* **2008**, *90*, 132–150.
- (60) Smith, J. N.; Dunn, M. J.; VanReken, T. M.; Iida, K.; Stolzenburg, M. R.; McMurry, P. H.; Huey, L. G. Chemical composition of atmospheric nanoparticles formed from nucleation in Tecamac, Mexico: Evidence for an important role for organic species in nanoparticle growth. *Geophys. Res. Lett.* **2008**, *35*.
- (61) Wang, L.; Khalizov, A. F.; Zheng, J.; Xu, W.; Ma, Y.; La, V.; Zhang, R. Atmospheric nanoparticles formed from heterogeneous reactions of organics. *Nat. Geosci.* **2010**, *3*, 238–242.